



ELSEVIER

Available online at [www.sciencedirect.com](http://www.sciencedirect.com)

SCIENCE @ DIRECT®

Earth and Planetary Science Letters 233 (2005) 17–32

EPSL

[www.elsevier.com/locate/epsl](http://www.elsevier.com/locate/epsl)

# In situ measurement of seasonal $\delta^{18}\text{O}$ variations and analysis of isotopic trends in a modern speleothem from southwest Australia

P.C. Treble<sup>a,b,\*</sup>, John Chappell<sup>b</sup>, Michael K. Gagan<sup>b</sup>,  
K.D. McKeegan<sup>a</sup>, T. Mark Harrison<sup>a,b</sup>

<sup>a</sup>Department of Earth and Space Sciences, University of California, Los Angeles, CA 90095-1567, USA

<sup>b</sup>Research School of Earth Sciences, The Australian National University, Canberra ACT 0200, Australia

Received 27 September 2004; received in revised form 20 January 2005; accepted 17 February 2005

Available online 29 March 2005

Editor: E. Bard

## Abstract

We present a record of seasonal and inter-annual oxygen ( $\delta^{18}\text{O}$ ) and carbon ( $\delta^{13}\text{C}$ ) isotope ratios from an 81-year-old stalagmite from Moondyne Cave, southwest Australia. The growth history of stalagmite MND-S1 is known since it grew on a cave boardwalk that was installed in 1911 and removed in 1992. This stalagmite provides an excellent test of speleothem climate proxies because the regional climate is strongly seasonal (wet winter/dry summer) and has experienced a 200 mm (20%) reduction of mean rainfall since the mid-1960s, and a 0.8 °C temperature rise since ~1953. Seasonal variations in calcite  $\delta^{18}\text{O}$  were measured in situ by high spatial resolution ion microprobe, whilst inter-annual variations of  $\delta^{18}\text{O}$  and  $\delta^{13}\text{C}$  were measured by conventional gas-source mass spectrometry.

Comparison of the speleothem stable isotopes and instrumental temperature records reveals that  $\delta^{18}\text{O}$  variations are too large to be driven by temperature alone, and are in the opposite sense. However, daily rainfall  $\delta^{18}\text{O}$  measurements show that the mean seasonal range in  $\delta^{18}\text{O}$  of rainfall in southwest Australia is large (2‰) and inversely correlated with rainfall amount. A rainfall driver for the speleothem  $\delta^{18}\text{O}$  is confirmed by the detection of seasonal shifts of 0.7–1.5‰ in speleothem  $\delta^{18}\text{O}$  that track rainfall  $\delta^{18}\text{O}$ , smoothed by storage in the overlying limestone. The seasonal range in speleothem  $\delta^{18}\text{O}$  is larger than any inter-annual and decadal variation observed in the record. The prominent annual cycles in speleothem  $\delta^{18}\text{O}$  revealed by ion microprobe analysis indicate that subtle changes in the frequency of intense winter rainfall events, or possibly also moisture sources, could produce significant changes in mean speleothem  $\delta^{18}\text{O}$ . The ion microprobe results also raise the possibility that the masses of speleothem calcite deposited in winter and summer could vary as a function of the seasonal drip rate and carbonate saturation state of these waters. If this is the case, then small changes in the relative masses of calcite deposited in winter and summer could produce significant shifts in mean  $\delta^{18}\text{O}$  and  $\delta^{13}\text{C}$  that have a complex relation to climate. This finding should be generally applicable to the interpretation of long-term trends in speleothem geochemical records for shallow cave

\* Corresponding author. Present address: Research School of Earth Sciences, The Australian National University, Canberra ACT 0200, Australia. Tel.: +61 2 6125 3406; fax: +61 2 6125 0738.

E-mail address: [pauline.treble@anu.edu.au](mailto:pauline.treble@anu.edu.au) (P.C. Treble).

sites where seasonal variations in geochemical tracers are relatively large, including most of the sub-tropical monsoon belts and mid to high latitudes with distinct rainfall seasons.

© 2005 Elsevier B.V. All rights reserved.

*Keywords:* speleothem; oxygen isotopes; carbon isotopes; annual cycle; rainfall; ion microprobe

## 1. Introduction

The stable isotopes of carbon ( $\delta^{13}\text{C}$ ) and oxygen ( $\delta^{18}\text{O}$ ) in speleothem carbonates are widely regarded as climate proxies and are routinely measured [1–7], yet few modern records exist to test their veracity against the instrumental climate record. This step is critical for understanding climate proxies, particularly those reflecting cumulative signals of complex processes. Speleothem  $\delta^{18}\text{O}$  records the combined signatures of rainfall  $\delta^{18}\text{O}$  and cave temperature, provided the calcite is precipitated in oxygen isotopic equilibrium [1]. Methods for separating the two effects, such as the analysis of fluid inclusions that represent the original drip water [8], are complicated and not routinely performed. Thus, many speleothem records are interpreted as combined records of rainfall and temperature [4,5], while some are recognised as being clearly dominated by rainfall [6].

Speleothem  $\delta^{13}\text{C}$  is also a composite signal, reflecting biogenic fractionation of the soil carbon pool [9], limestone dissolution under open- or closed-system conditions [10,11], prior carbonate precipitation from groundwater [12], and the rate of  $\text{CO}_2$  degassing from drip waters over a speleothem surface [10,11]. The term open system or closed system refers to limestone dissolution conditions where groundwaters either remain in contact with soil  $\text{CO}_2$  (open) or are isolated from soil  $\text{CO}_2$  (closed) after acidification [11]. Biogenic  $\text{CO}_2$  produced under C3 vegetation has an average  $\delta^{13}\text{C}$  value of  $-27\text{‰}$ , but may vary by approximately  $\pm 5\text{‰}$  depending on the environmental effects on photosynthesis [13,14]. Soil  $\text{CO}_2$  is dominated by biogenic  $\text{CO}_2$  but can be mixed with atmospheric  $\text{CO}_2$  when soil respiration rates are low [15]. The contribution of carbon atoms from limestone dissolution is negligible under open-system conditions and small under closed-system conditions [11,16]. By contrast, degassing of  $\text{CO}_2$  before drip water reaches the speleothem, and the subsequent conversion of  $\text{HCO}_3^-$  to  $\text{CO}_{2(\text{aq})}$ , may substantially

raise the  $^{13}\text{C}/^{12}\text{C}$  of the precipitating solution. This may be driven by a reduction in the partial pressure of  $\text{CO}_2$  in drip waters when they enter the cave [11,16], or because calcite has been lost from solution in aquifer pore spaces or over other formations (prior calcite precipitation) [12].

A critical factor in interpreting speleothem  $\delta^{13}\text{C}$  and  $\delta^{18}\text{O}$  records is determining whether disequilibrium isotopic fractionation caused by rapid  $\text{CO}_2$  degassing or, rarely, by evaporation of the precipitating solution [11], overprints climatic signals. Isotopic disequilibrium is indicated by a simultaneous increase of  $\delta^{13}\text{C}$  and  $\delta^{18}\text{O}$  down a growth layer from the speleothem apex, and by correlation between  $\delta^{13}\text{C}$  and  $\delta^{18}\text{O}$  along a growth axis [11]. This is because  $\delta^{13}\text{C}$  and  $\delta^{18}\text{O}$  are affected simultaneously if the removal of  $\text{CO}_{2(\text{g})}$  outpaces the conversion of  $\text{CO}_{2(\text{aq})}$  to  $\text{HCO}_3^-$  [11]. However, these tests tend not to be definitive in practice because it is almost impossible to sample coeval calcite along a growth layer. Moreover, climatic factors conceivably can simultaneously affect axial profiles of both speleothem  $\delta^{18}\text{O}$  and  $\delta^{13}\text{C}$ .

To improve our understanding of isotopes in speleothems, we examined seasonal variations of  $\delta^{18}\text{O}$ , and inter-annual variations of  $\delta^{18}\text{O}$  and  $\delta^{13}\text{C}$  in a modern speleothem of known growth history. Our test sample is a 33 mm tall, 59 mm wide stalagmite (MND-S1) that grew from 1911 to 1992 on a boardwalk in Moondyne Cave, southwest Western Australia ( $34^\circ 16'\text{S}$ ,  $115^\circ 05'\text{E}$ ; Fig. 1). The calcite crystal fabric of MND-S1 is columnar palisade [17], with inclusions between crystallites preserved in the mid-section (open columnar palisade fabric; 1930–1970), and dense, compact inclusion-free (closed columnar palisade fabric) calcite above and below this (Fig. 2).

Stalagmite MND-S1 preserves clear trace element cycles (P, Mg, U, Sr, Ba, and Na) previously analysed by excimer laser ablation inductively coupled plasma mass spectrometry (ELA-ICPMS) [18]. These cycles were determined to be annual based on the agreement between the number of cycles in MND-S1 and the

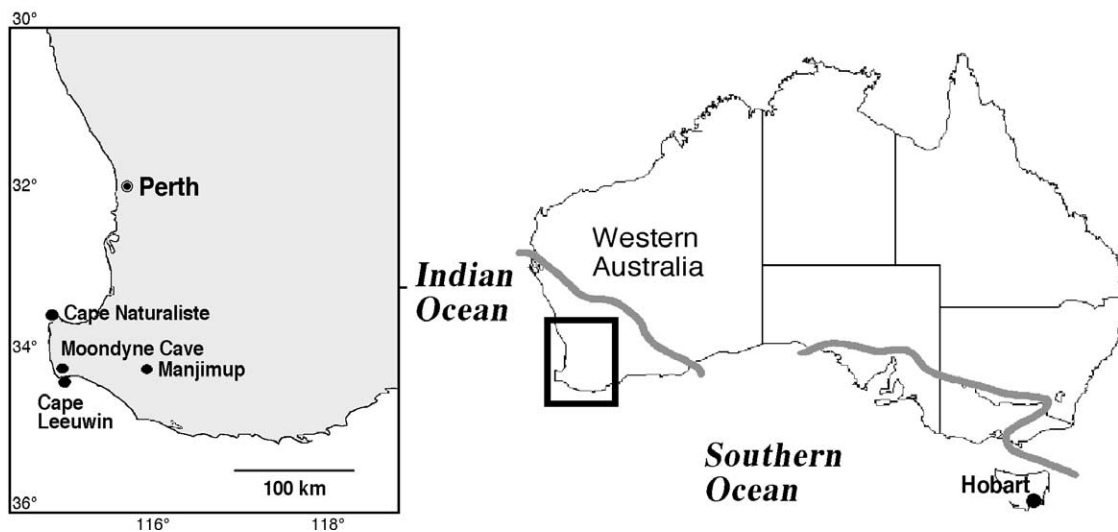


Fig. 1. Location of stalagmite MND-S1 (Moondyne Cave), rainfall collection site (Cape Leeuwin), Cape Naturaliste, and high-quality instrumental climate dataset (Manjimup) in southwest Western Australia. A long and detailed study of rainfall  $\delta^{18}\text{O}$  was conducted at Hobart, Tasmania. Area south of thick grey line is Australia's winter rainfall zone.

number of years that the boardwalk was in the cave [18]. Thus the chronology of MND-S1 is well-known, constrained by the time the boardwalk was in place (1911–1992) and the yearly markers provided by the annual trace element cycles. The trace element cycles represent seasonal variations in the chemistry of meteoric water as it passes through, and interacts with, the soil and limestone. No detailed study of aquifer hydrology was undertaken, but the presence of seasonal trace element variations led us to expect that seasonal variations in rainwater  $\delta^{18}\text{O}$  will be preserved

also. We used high-resolution in situ ion microprobe analysis to investigate this possibility, and hence that rainfall is the primary driver of  $\delta^{18}\text{O}$  in MND-S1.

## 2. Environmental setting

Moondyne Cave is a syngenetic karst cavern developed in Late Cenozoic calcarenite and aeolianite limestone [19], with a relatively thin roof (15–20 m) beneath a *Eucalyptus* forest. Total cave length is 170

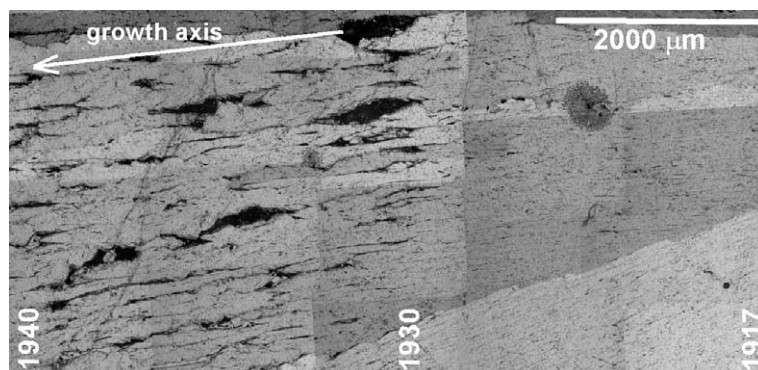


Fig. 2. Thin-section photograph of stalagmite MND-S1 under cross-polarised light showing the transition from compact, inclusion-free columnar fabric to inclusion-rich columnar fabric at ~1930. The photograph spans ~1917 to ~1940. The abrupt change in growth fabric coincides with the 0.3‰ increase in speleothem  $\delta^{18}\text{O}$  at 1930.

m and MND-S1 was located approximately 60 m from the cave entrance (approximately  $1.5 \times 1.5$  m wide). The cave is located 3 km from the coast in a temperate climate with predominantly winter rainfall. Average annual rainfall at the nearest station, Cape Leeuwin Lighthouse (12 km from Moondyne Cave; Fig. 1), is 1010 mm. 798 mm/year is recorded at Manjimup station (97 km inland from Moondyne Cave; Fig. 1) where the nearest high quality climate dataset is available [20]. Average annual surface air temperatures at Cape Leeuwin range from 13.8 °C in July–August to 20.3 °C in January–February, which is much larger than the annual temperature range where MND-S1 grew ( $15.9\text{--}16.5 \pm 0.2$  °C), recorded by data logger measurements at 4-h intervals for 1 year. The 0.6 °C seasonal cycle in cave temperature lags the surface air temperature by approximately 3 months, owing to the insulation provided by the limestone. The average daily temperature range at the lighthouse is approximately 5–6 °C, but no diurnal temperature variations were recorded in the cave, indicating minimal air circulation at the site of MND-S1.

The area above Moondyne Cave was reasonably free of activities that would have greatly disturbed the soil and catchment owing to the hilly topography of the limestone ridge, although the area was regularly burnt to reduce the understorey of the *Eucalyptus* forest to allow cattle passage. The forest understorey may have thickened through time in response to less frequent burning when large tracts of land, including that over Moondyne Cave, were incorporated into the Leewin–Naturaliste National Park in about 1980 (S. Eberhard, personal communication). Moondyne Cave was used for cave tours until 1959 and was closed until 1992 when it underwent restoration, and the boardwalk on which MND-S1 grew was removed. No detailed records of tourist numbers exist between 1911 and 1959 when tours were operated, but we believe that tours were infrequent as tourists had to first collect the guide from Augusta, 10 km from the cave.

Regional meteorologic records show that mean winter temperature has risen by 0.8 °C since 1954, and rainfall has decreased by about 200 mm (20%) since 1965–1970 [21]. This has resulted in a 42% decrease of streamflow into water storages. Consequently, the city of Perth and the surrounding region face a critical shortfall of water. Palaeo-rainfall records that extend climate data beyond the instru-

mental records are needed to understand the nature of this climatic change. Hence, it is important to fully evaluate the potential for reconstructing rainfall variations from speleothem oxygen and carbon isotope records.

The oxygen isotopic composition of rainfall is known to vary both in time and space [22] and can strongly influence speleothem  $\delta^{18}\text{O}$  when the seasonal variation is large [6]. To determine the seasonal variation of  $\delta^{18}\text{O}$  in southwest Australian rainfall, we also present a 1 year (October 2000–October 2001) time series of rainfall  $\delta^{18}\text{O}$  using samples collected on a daily basis at Cape Leeuwin Lighthouse. This collection would have been ideally complemented by weekly or monthly cave drip water sampling over the same time period; however, it was not possible to collect drip water, apart from on one occasion in June 2002, owing to cave access restrictions.

### 3. Methods

#### 3.1. $\delta^{18}\text{O}$ analysis of rainfall

Rainfall samples were caught in a clean high-density polyethylene bottle fitted with a funnel and ball valve and collected between 8 and 9 a.m. after rain fell during the previous 24 h, between October 20, 2000 and October 12, 2001, except on four occasions when the rain was collected after 48 h.  $\delta^{18}\text{O}$  measurements were conducted on samples for which at least 1 mm of rain fell. The  $\delta^{18}\text{O}$  values of rainfall collected between October 2000 and May 2001 were measured in duplicate at the Research School of Biological Sciences, ANU, using an on-line pyrolysis technique [23]. Twenty-six measurements of the in-house ANU-HP1 water standard ( $-5.54\text{‰}_{\text{VSMOW}}$ ) yielded a precision of  $\pm 0.5\text{‰}$  ( $2\sigma$ ). The  $\delta^{18}\text{O}$  values of rainfall collected between June 2001 and October 2001 were measured off-line at the Research School of Earth Sciences (RSES), ANU, following a modified version of the  $\text{H}_2\text{O}\text{--CO}_2$  equilibration technique [24] described by Socki et al. [25]. Two-millilitre water samples were equilibrated with 8 ml of  $\text{CO}_2$  gas of known isotopic composition at  $25.0 \pm 0.1$  °C for a minimum of 40 h. The equilibrated  $\text{H}_2\text{O}\text{--CO}_2$  gas was then injected into a vacuum line for  $\text{CO}_2$  extraction. The  $\delta^{18}\text{O}$  value of the purified  $\text{CO}_2$  was measured on

a Finnigan MAT-251 mass spectrometer and expressed relative to Vienna Standard Mean Ocean Water (VSMOW). Nine measurements of ANU-HP1 yielded a precision of  $\pm 0.04\text{‰}$  ( $2\sigma$ ). Measurements of two unknowns using both the pyrolysis and  $\text{CO}_2$  equilibration techniques were within  $0.5\text{‰}$ .

The rainfall  $\delta^{18}\text{O}$  data were compared with daily rainfall totals and mean, maximum and minimum surface temperatures recorded during each 24-h collection period at the lighthouse. Partial correlation coefficients are presented to determine the relationship between  $\delta^{18}\text{O}$  and rainfall or temperature with the influence of the inter-related rainfall and temperature variables removed ( $r = -0.22$ ,  $p < 0.05$ , for the raindays examined).

### 3.2. Analysis of speleothem $\delta^{18}\text{O}$ and $\delta^{13}\text{C}$ by conventional techniques

A 5 mm thick slice was cut from the central growth axis of stalagmite MND-S1 and then halved along the growth axis. Carbonate powders were milled in a continuous fashion along the cut edge of the growth axis using a 2 mm diameter tungsten carbide end-mill bit, effectively shaving approximately 1 mg of powder at 0.5 mm increments. This sampling technique fully integrates the isotopic signal for every 0.5 mm increment of growth, as opposed to the more common method of sampling speleothems by drilling isolated holes. The technique adopted here is preferable when potentially large  $\delta^{18}\text{O}$  variations over short intervals, such as seasonal variations, are anticipated. Full details of the method are given in Gagan et al. [26]. 200- $\mu\text{g}$  sub-samples were reacted with anhydrous  $\text{H}_3\text{PO}_4$  in a Kiel microcarbonate preparation device at  $90^\circ\text{C}$ , equivalent to the McCrea method [27]. The evolved  $\text{CO}_2$  gas was measured in a Finnigan MAT 251 mass spectrometer at RSES, ANU. Data are normalised to the Vienna Peedee Belemnite (VPDB) scale using National Bureau of Standards NBS-19 ( $\delta^{18}\text{O} = -2.20\text{‰}$  and  $\delta^{13}\text{C} = +1.95\text{‰}$ ). The long-term measurement precision for NBS-19 at RSES is  $\pm 0.07\text{‰}$  ( $2\sigma$ ) for  $\delta^{18}\text{O}$  and  $\pm 0.04\text{‰}$  ( $2\sigma$ ) for  $\delta^{13}\text{C}$ .

### 3.3. Ion microprobe analysis of seasonal $\delta^{18}\text{O}$

Annual cycles of trace elements in MND-S1 have an average length of  $\sim 370\ \mu\text{m}$  [18], which is wide

enough to permit sub-annual sampling by micro-shaving techniques [28] (e.g., every  $30\ \mu\text{m}$  along the growth axis). However, to obtain the  $200\ \mu\text{g}$  of powder required for analysis, the speleothem must be shaved deeper along the layers, perpendicular to the growth axis ( $1.4 \times 1.4\ \text{mm}$ ). This technique is only suitable if the growth layers are parallel to avoid smoothing the signal by sample averaging. We observed from secondary electron microscopy images [29] that the annual growth layers in MND-S1 are not simple parallel structures, but vary in thickness and occasionally pinch-out. This complex growth precludes the accurate analysis of annual cycles by the micro-shaving techniques described. We also point-out that 100% recovery of finely powdered material is difficult, and much smaller amounts would actually be recovered (50–100  $\mu\text{g}$ ), reducing the analytical precision. As the micro-shaving techniques would average the MND-S1  $\delta^{18}\text{O}$  signal, we employed high spatial resolution in situ ion microprobe techniques to measure sub-annual  $\delta^{18}\text{O}$ . Sputter craters from ion microprobe techniques are  $\sim 20\text{--}30\ \mu\text{m}$  in diameter and  $1\text{--}2\ \mu\text{m}$  deep.

In situ  $\delta^{18}\text{O}$  was measured on a Cameca IMS-1270 ion microprobe at the University of California, Los Angeles. Polished Au-coated samples were sputtered with a 2–3 nA  $\text{Cs}^+$  primary beam to produce negative secondary ions at mean intensities of approximately  $3 \times 10^9$  cps ( $^{16}\text{O}$ ) and  $6 \times 10^6$  cps ( $^{18}\text{O}$ ). The  $^{18}\text{O}^-$  and  $^{16}\text{O}^-$  ion beams were collected simultaneously in Faraday cups after pre-sputtering the analytical area for 180 s to achieve sputtering equilibrium. Signals were measured for 100 s (collected in 10 blocks of 10 s integration time), which yielded a typical internal counting precision of  $\pm 0.1\text{‰}$  ( $2\sigma$ ). The  $^{16}\text{O}$  and  $^{18}\text{O}$  intensities were maintained within a narrow range to avoid potential need to correct for non-linear detector response. Background current measurements were made for every 10 unknowns by blocking the  $\text{Cs}^+$  beam and subtracting from sample measurements.

The analytical precision of ion microprobe measurements of  $\delta^{18}\text{O}$  in individual grains was  $\pm 0.7\text{‰}$  ( $2\sigma$ ,  $n = 14$ ) for NBS-19 and  $\pm 0.5\text{‰}$  ( $2\sigma$ ,  $n = 8$ ) for NBS-18. In principle, this level of uncertainty could reflect the inherent instability of the ion microprobe analyses with respect to reproducibility of instrumental mass discrimination. However, isotopic heterogeneities of NBS-19 and NBS-18 at the spatial scale

of ion microprobe analyses may also contribute to the observed variability. To test this idea, we performed closely spaced in situ  $\delta^{18}\text{O}$  analyses on a petrographic glass slide. The results showed that the ion microprobe can produce repeat measurements with a precision of  $\pm 0.4\text{‰}$  ( $2\sigma, n=7$ ), once stable running conditions are achieved, on a (presumably) homogeneous sample with a near-perfectly flat geometry.

Regardless of whether the variations in the analyses of NBS-19 or NBS-18 can be attributed to isotopic heterogeneity, or geometric imperfections caused by the mounting and polishing of small NBS-19 and NBS-18 grains in epoxy, we considered these to be unsuitable standard materials for calibration of unknowns with small isotopic variations, such as speleothems. The isotopically homogeneous petrographic glass slide is useful for monitoring potential measurement drift but cannot be used to standardise speleothem  $\delta^{18}\text{O}$  owing to possible matrix effects between dissimilar materials. Therefore, the means of all in situ measurements of  $\delta^{18}\text{O}$  in each transect were corrected to the bulk mean  $\delta^{18}\text{O}$  value determined from conventional analyses (e.g., [30]). While the accuracy of  $\delta^{18}\text{O}$  values (relative to VPDB or VSMOW) is of secondary importance for our investigation, this standardisation procedure effectively improves measurement reproducibility [30], thus permitting resolution of isotopic variations intrinsic to the sample. The difference of  $21.8 \pm 0.9\text{‰}$  in  $\delta^{18}\text{O}$  between NBS-19 and NBS-18, measured by the UCLA ion microprobe, is close to the accepted difference of  $20.8\text{‰}$ , so no adjustment to the relative instrumental mass discrimination was necessary.

Analytical spots were arranged in a zig-zag pattern (Fig. 3) along the speleothem growth axis to max-

imise spatial resolution across the fine-scale growth bands. Sputter ablation pits were kept  $\sim 30\ \mu\text{m}$  apart to avoid undesirable topographic effects on the trajectories of charge-neutralising electrons, as well as  $\text{Cs}^+$  and  $\text{O}^-$  ions. The positioning of each ion probe sputter crater was determined using a Mitutoyo profile projector with the digital readout on the  $x$ - $y$  stage reproducible to  $\pm 2\ \mu\text{m}$ . The relationship between  $\delta^{18}\text{O}$  and trace element variations was established by measuring trace elements by ELA-ICPMS, effectively scanning directly across the transects of in situ  $\delta^{18}\text{O}$  pits with a  $32\ \mu\text{m}$  spot as described previously [18]. This technique produced trace element concentration data measured over the same transect and thus is accurately registered spatially with the ion microprobe  $\delta^{18}\text{O}$  data. In order to compare the conventional and in situ isotope data, an age model was constructed for the conventional  $\delta^{18}\text{O}$  record using the annual Ba cycles measured by ELA-ICPMS along the cut edge that was created when the conventional samples were milled.

## 4. Results and discussion

### 4.1. Rainfall $\delta^{18}\text{O}$

Strong seasonality in rainfall  $\delta^{18}\text{O}$  is evident in the Cape Leeuwin Lighthouse record (Fig. 4A) with precipitation-weighted  $\delta^{18}\text{O}$  lower in wet winter months ( $-4.7\text{‰}$ , May–September; October incompletely sampled) and higher in dry summer months ( $-2.7\text{‰}$ , November–April). Overall, the precipitation-weighted mean  $\delta^{18}\text{O}$  value is  $-4.3\text{‰}$ . Fig. 4B shows rainfall and  $\delta^{18}\text{O}$  data grouped by months with

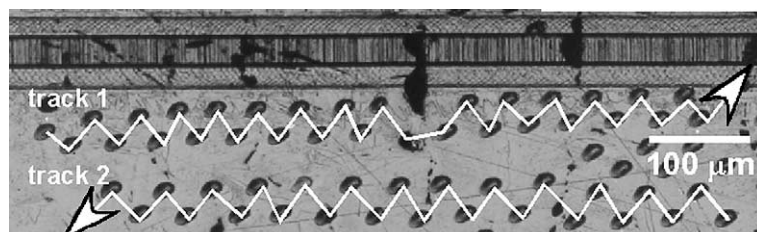


Fig. 3. Arrangement of ion microprobe ablation pits on stalagmite MND-S1. Individual measurements were positioned in a zig-zag pattern to increase the spatial resolution of the record. Arrows indicate the direction of measurements. Trace element variations were later measured directly over the ion microprobe pits by laser ablation along each of transects 1 and 2. Transect 3 (not shown) is located 1.5 mm from, and parallel to, transects 1 and 2.

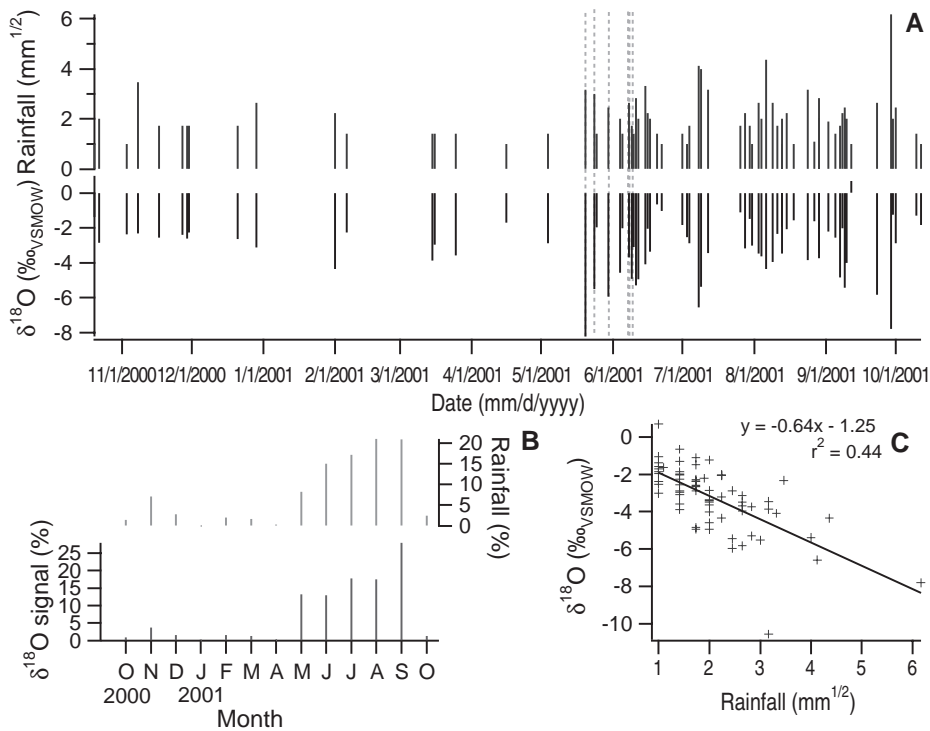


Fig. 4. Comparison of the square root of rainfall amount and  $\delta^{18}\text{O}$  of rainfall in southwest Australia. (A) Daily rainfall  $\delta^{18}\text{O}$  measurements at lighthouse from October 20, 2000 to October 12, 2001. The mean  $\delta^{18}\text{O}$  of winter rainfall (May–October) is 2‰ lower than the that for summer rainfall (November–April). Dashed lines show rainfall events associated with meridional troughs identified from mean sea-level pressure and cloud cover synoptic charts. (B) Data grouped into months and expressed as a portion of the yearly rainfall and  $\delta^{18}\text{O}$  values demonstrating the dominant winter signal. Monthly  $\delta^{18}\text{O}$  expressed as a percentage is  $\frac{\sum(\delta^{18}\text{O}_i \times \text{rainfall}_i)}{\text{total rainfall collected}} \div \text{mean } \delta^{18}\text{O}_{\text{precipitation-weighted}} \times 100$ , where  $i_1, i_2, i_3, \dots, i_n$  per month and  $n$ =number of events per month. (C) Cross-plot showing non-linear inverse relationship between rainfall amount and rainfall  $\delta^{18}\text{O}$ .

both variables expressed as the percentage each month contributes to the overall signal in the October 2000–October 2001 dataset. This exercise further reveals the strong seasonal rainfall  $\delta^{18}\text{O}$  cycle and demonstrates that the majority of drip water  $\delta^{18}\text{O}$  will be derived from May to September rainfall.

The partial correlation coefficient between  $\delta^{18}\text{O}$  and rainfall amount is higher ( $r = -0.60$ ;  $p < 0.01$ ) than that for mean, maximum, or minimum surface temperatures ( $r = 0.03$ – $0.14$ ) based on the daily data. The relationship between rainfall amount and  $\delta^{18}\text{O}$  is inverse and non-linear over the large range of daily rainfall sampled (1–38 mm), with heavier rainfall events (10 mm or more) being relatively isotopically enriched. If the square root of rainfall amount is taken (Fig. 4C), the partial correlation coefficient between that parameter and rainfall  $\delta^{18}\text{O}$  is  $-0.66$  ( $p < 0.01$ ).

An inverse relationship with rainfall amount and no significant relationship between rainfall  $\delta^{18}\text{O}$  and surface temperature is consistent with the findings for a 5-year event-based rainfall  $\delta^{18}\text{O}$  record [31] from Hobart, Tasmania, in southeastern Australia (location: Fig. 1). Both sites lie in the path of the same mid-latitude low-pressure systems and fronts that first cross or pass south of southwest Australia, then cross Tasmania a few days later. In Tasmania, rainfall  $\delta^{18}\text{O}$  varies inversely with rainfall amount, and both variables are closely related to the prevailing synoptic conditions, driven by the intensity and proximity of low pressure systems in the Southern Ocean [31]. Large amounts of isotopically lighter rain are delivered when these systems pass close to the coast of southern Australia, whereas lesser amounts of isotopically heavier rain are delivered from weaker frontal

rainfall generated when these systems pass far to the south of Australia [31]. This trend is driven by the intense convective and recycling processes in these cyclonic systems such that the  $^{18}\text{O}/^{16}\text{O}$  ratio is lowest at the core compared with frontal rainfall produced further from the centre, where atmospheric convection is less intense [32].

#### 4.2. In situ ion microprobe $\delta^{18}\text{O}$ : seasonal climatic signals

Two parallel transects of in situ ion microprobe measurements of  $\delta^{18}\text{O}$  from a 2 mm section of MND-S1 (~45 measurements per track) equivalent to ~6 yr growth are shown in Fig. 5A, and conventional  $\delta^{18}\text{O}$  analyses from the same interval in Fig. 5B. The four conventional analyses vary by only 0.2‰, whereas  $\delta^{18}\text{O}$  for the microprobe tracks varies

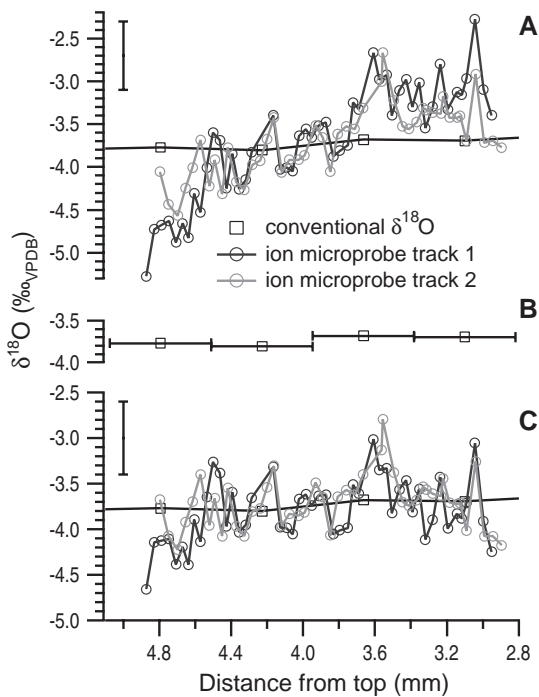


Fig. 5. Comparison of ion microprobe  $\delta^{18}\text{O}$  and conventional  $\delta^{18}\text{O}$  records for stalagmite MND-S1. (A) Ion microprobe  $\delta^{18}\text{O}$  demonstrating reproducibility for two adjacent transects on MND-S1. (B) Conventional  $\delta^{18}\text{O}$  record is shown for comparison. (C) Ion microprobe  $\delta^{18}\text{O}$  after correcting for geometric error. These data show three to four reproducible cycles between 3.5 mm and 4.7 mm. Bar indicates  $2\sigma$  uncertainty.

from about  $-2.7\text{‰}$  to  $-4.8\text{‰}$ . The long-term trend in the ion microprobe data is  $1\text{‰}$  compared with  $0.2\text{‰}$  for the conventionally measured data. This discrepancy cannot be due to temporal analytical drift as tracks 1 and 2 were acquired in opposite directions (Fig. 3), which suggests that a systematic error due to sample geometry was responsible. Subtle relief between the speleothem and surrounding epoxy resin, due to polishing of dissimilar materials, can affect instrumental mass fractionation by altering secondary ion optics and the charge neutralisation balance at the sample edge [33]. The trend in the microprobe  $\delta^{18}\text{O}$  record was corrected to  $0.2\text{‰}$  by subtracting an extrapolated linear correction for each transect (Fig. 5C).

Although somewhat noisy, the patterns in  $\delta^{18}\text{O}$  for both microprobe tracks are similar. The  $\pm 0.4\text{‰}$  ( $2\sigma$ ) error bar for the microprobe  $\delta^{18}\text{O}$  data in Fig. 5A and C is based on the measurement reproducibility for a glass slide and demonstrates that some of the high frequency  $\delta^{18}\text{O}$  variability in MND-S1 is within analytical uncertainty. However, the three  $\delta^{18}\text{O}$  cycles between 3.5 and 4.4 mm in Fig. 5C are clearly reproduced in both microprobe transects. Another  $\delta^{18}\text{O}$  cycle between 4.5 and 4.7 mm is reproduced, but appears to be somewhat asynchronous. The wavelengths of these cycles (0.3–0.4 mm) are similar to the average annual trace element wavelength (0.37 mm).

Fig. 6 shows ion microprobe  $\delta^{18}\text{O}$  data for a third, longer transect located further from the sample edge, 1.5 mm away from and parallel to transects 1 and 2. The ion microprobe and conventional  $\delta^{18}\text{O}$  records are in agreement, with neither showing any overall trend, indicating that transect 3 was not affected by geometric effects. Transect 3  $\delta^{18}\text{O}$  data are shown in parallel with Ba and Mg, which vary seasonally with low Ba and high Mg in summer [18]. Judged from the Ba master record constructed for MND-S1 [18], transect 3 spans years 1975–1985 AD. Variations of microprobe  $\delta^{18}\text{O}$  in Fig. 6 can be matched visually to trace element cycles at several points, but agreement is weaker than that between the trace element cycles themselves. Where agreement is clear,  $\delta^{18}\text{O}$  maxima correspond to high Mg and low Ba in summer, whereas  $\delta^{18}\text{O}$  minima correspond to low Mg and high Ba in winter (e.g., years 1979 and 1980). The amplitudes of the most regular  $\delta^{18}\text{O}$  cycles are  $\sim 0.7\text{‰}$ –

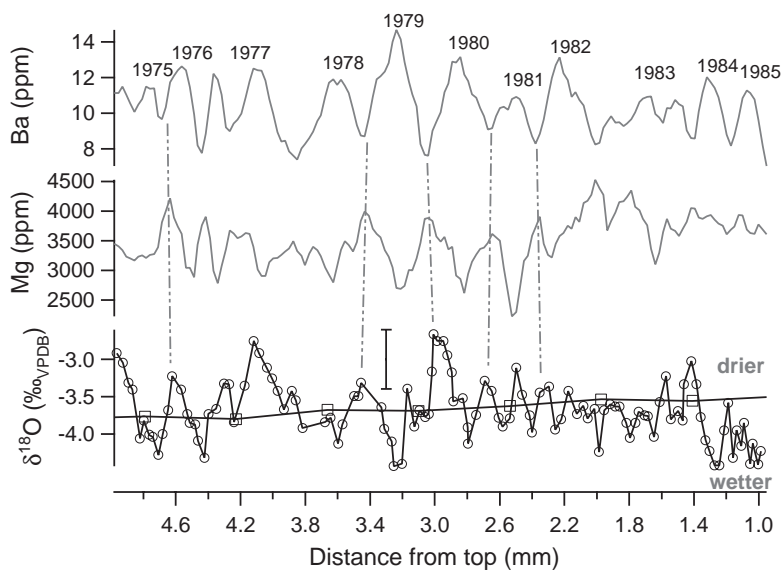


Fig. 6. Comparison of a third ion microprobe  $\delta^{18}\text{O}$  transect (circles), conventional  $\delta^{18}\text{O}$  record (squares), and annual cycles of Ba and Mg measured by ELA-ICPMS [18] over the same section on MND-S1 (~1975–1985).  $\delta^{18}\text{O}$  peaks correspond with Mg peaks and Ba troughs (dashed lines) when prominent annual cycles are present in the signals. Bar indicates  $2\sigma$  uncertainty for microprobe  $\delta^{18}\text{O}$ .

1.5‰. However, some years show more than one  $\delta^{18}\text{O}$  peak (e.g., 1981 and 1982), and major  $\delta^{18}\text{O}$  maxima do not always coincide with Ba minima (e.g., 1977).

We consider that a major source of the speleothem  $\delta^{18}\text{O}$  variation lies in seasonal variation of the isotopic composition of rainfall, driven primarily by rainfall amount and not by surface temperature. Given that the observed seasonal temperature variation in Moondyne Cave is only 0.6 °C, the seasonal difference in the temperature-dependent fractionation of  $^{18}\text{O}/^{16}\text{O}$  in speleothem calcite will be negligible ( $\sim 0.14\text{‰}$  based on  $-0.23\text{‰}/^\circ\text{C}$ ; [34]). Moreover, if the temperature-dependent fractionation effect was dominant, speleothem calcite  $\delta^{18}\text{O}$  would tend to be lower in summer than in winter, which is opposite to the observed pattern. Thus the tendency for  $\delta^{18}\text{O}$  in MND-S1 to be lower in winter is consistent with the relationship between rainfall amount (wetter in winter) and rainfall  $\delta^{18}\text{O}$  (lower in winter) deduced from measurements of  $\delta^{18}\text{O}$  in local rainfall (Fig. 4A–C).

The seasonal range of  $\delta^{18}\text{O}$  in Moondyne Cave drip water is not known. However, it is likely to be smaller than the 2‰ seasonal range in rainfall  $\delta^{18}\text{O}$ , as is observed for shallow caves elsewhere in southern

Australia [35], presumably because seepage-fed components dominate over fracture-fed components (e.g., [36]), resulting in smoothing of the rainfall  $\delta^{18}\text{O}$  cycle. The 0.7–1.5‰ cycles in speleothem  $\delta^{18}\text{O}$  are consistent with the range expected for a smoothed seasonal cycle of rainfall  $\delta^{18}\text{O}$ . Finally, it is not unexpected that trace element cycles, which essentially follow the seasonal cycle of rainfall [18], are more regular than  $\delta^{18}\text{O}$  variations, which reflect the complex mixture of the isotopic signatures of individual rainfall events. This is a noisy process. Fig. 4A shows that event-to-event  $\delta^{18}\text{O}$  values can vary by as much as 6–7‰.

#### 4.3. Inter-annual speleothem $\delta^{18}\text{O}$ and $\delta^{13}\text{C}$ : complex responses to climate

The inter-annual  $\delta^{18}\text{O}$  and  $\delta^{13}\text{C}$  data are shown alongside the instrumental temperature and rainfall records in Fig. 7. The  $\delta^{13}\text{C}$  values are relatively constant at  $-9\text{‰}$  between 1912 and 1925, and decrease to  $-10\text{‰}$  by 1935.  $\delta^{13}\text{C}$  values increase towards the present, with minor lows at 1950, 1965, and 1974, to reach  $-7.7\text{‰}$  in 1992. Speleothem  $\delta^{18}\text{O}$  values began at  $-3.8\text{‰}$  in 1912, then increased to  $-3.5\text{‰}$  in 1992 and showed several inter-annual

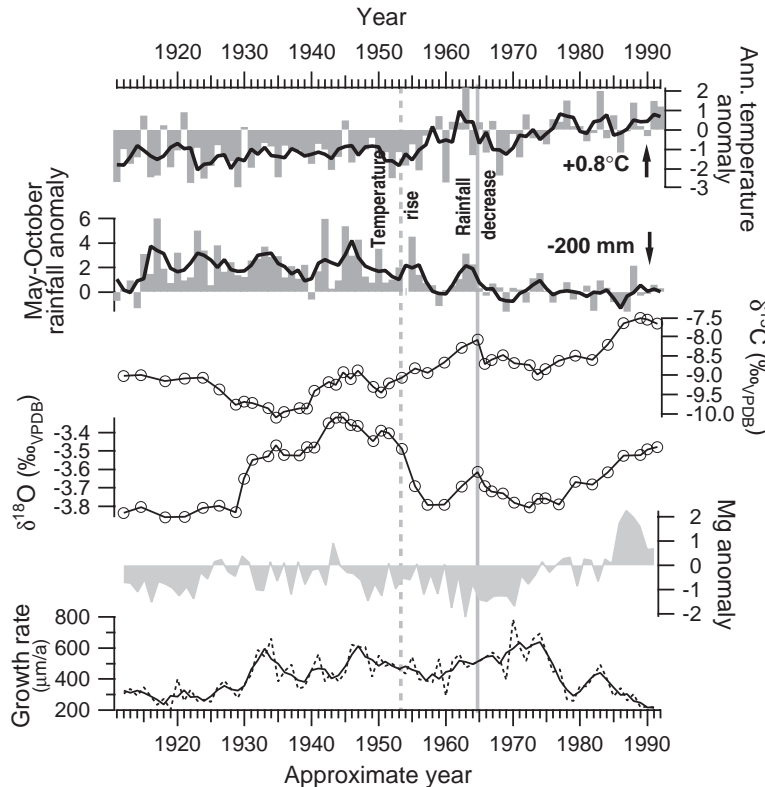


Fig. 7. Comparison of annual temperature, May–October rainfall, conventional  $\delta^{13}\text{C}$  and  $\delta^{18}\text{O}$ , speleothem Mg [18], and speleothem growth rate for MND-S1. Black curves show the three-point running means. Instrumental temperature, rainfall (Manjimup dataset [20]), and Mg anomalies are calculated by subtracting the mean and dividing by the standard deviation of the period 1965–1992 (units are standard deviation). Annual average temperature has increased by  $0.8\text{ }^{\circ}\text{C}$  since 1953 while winter rainfall has decreased by 200 mm since 1964 in the Manjimup record. Growth rate is shown as the yearly wavelength (dashed curve) and 3-yr running mean (solid curve) of a master trace element record compiled from 11 ELA-ICPMS transects on MND-S1 [18]. The growth rates differ slightly from those published previously [18] as this curve was determined using the distance over successive 5-yr intervals.

variations that mimic details of the  $\delta^{13}\text{C}$  record. However, there is a significant positive shift of  $0.3\text{--}0.5\text{‰}$  between 1930 and 1955 that is not mirrored in  $\delta^{13}\text{C}$ . This  $\delta^{18}\text{O}$  plateau was confirmed by repeat measurements. There is no significant correlation between  $\delta^{13}\text{C}$  and  $\delta^{18}\text{O}$  when all the data are considered ( $r = -0.1$ ;  $n = 44$ ). But, if the 1930–1955 period is considered separately, the year-to-year covariation is quite strong:  $r = +0.75$  ( $p < 0.001$ ;  $n = 26$ ) across the  $\delta^{18}\text{O}$  plateau and  $+0.92$  ( $p < 0.01$ ;  $n = 16$ ) for the data prior to and after the plateau (Fig. 8), implying that isotopic disequilibrium cannot be ruled out as a cause of minor variation. However, disequilibrium cannot be the cause of the high  $\delta^{18}\text{O}$  values from 1930 to 1955 because  $\delta^{13}\text{C}$  is

lower during this interval than at any time before or since.

Neither  $\delta^{13}\text{C}$  nor  $\delta^{18}\text{O}$  shows simple responses to variations in mean annual temperature or rainfall. Overall,  $\delta^{13}\text{C}$  increased by  $2.5\text{‰}$  from 1938 to 1992 (Fig. 7). The beginning of this rise precedes both the temperature increase and the rainfall decrease by 15 and 27 yr, respectively. The  $\delta^{18}\text{O}$  variations in MND-S1 are unrelated to temperature: the positive shift from 1930 to 1955 occurs when mean annual temperature is virtually constant, and the increase in  $\delta^{18}\text{O}$  since 1970 is in the opposite sense to the isotopic effect of the observed recent warming. Moreover, the ion microprobe data indicate that speleothem  $\delta^{18}\text{O}$  is driven primarily by rainfall. The timing of the post-1970 rise

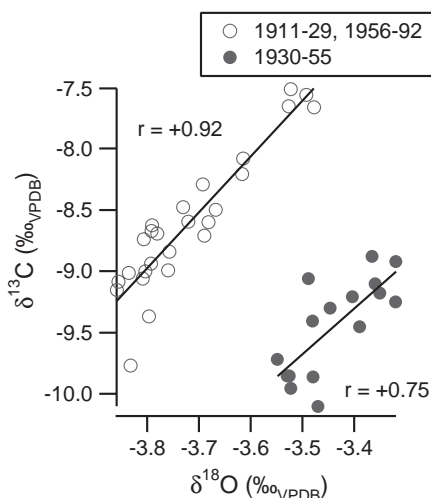


Fig. 8. Comparison of conventional analyses of  $\delta^{18}\text{O}$  and  $\delta^{13}\text{C}$  for the  $\delta^{18}\text{O}$  plateau (1930–1955) and the periods before and after the plateau (1911–1929, 1956–1992). The  $\delta^{18}\text{O}$  and  $\delta^{13}\text{C}$  values for the two data clusters show a clear offset, but are otherwise highly correlated. The linear least squares regression equations are  $\delta^{13}\text{C}=3.7\delta^{18}\text{O}+3.3$  for the plateau and  $\delta^{13}\text{C}=4.5\delta^{18}\text{O}+8.3$  for the periods before and after the plateau.

in  $\delta^{18}\text{O}$  is coincident with an increase in speleothem Mg (Fig. 7) and decrease in speleothem P (not shown) [18], which were interpreted previously to be rainfall-sensitive trace elements [18].

#### 4.4. Isotopic disequilibrium processes

A key concern when reconstructing climate using speleothem isotope records is determining whether speleothem  $\delta^{18}\text{O}$  and/or  $\delta^{13}\text{C}$  is affected by disequilibrium processes. The high covariation between these variables along the growth axis in MND-S1 (Figs. 7 and 8) indicates that kinetic processes may be driving the sub-decadal variability. This is further supported by the slope of the linear regressions (Fig. 8), which indicates that the variation in  $\delta^{13}\text{C}$  is 3.7 times that of  $\delta^{18}\text{O}$  during the plateau period, and 4.5 before and after. This variation is close to the ratio 3:1 proposed by Hendy [11] to indicate isotopic disequilibrium, reflecting the simultaneous but larger effect on  $\delta^{13}\text{C}$  versus  $\delta^{18}\text{O}$ .

Isotopic disequilibrium is also indicated by a simultaneous increase of  $\delta^{13}\text{C}$  and  $\delta^{18}\text{O}$  down a growth layer from the speleothem apex [11]. This test

is less subjective in principle, but not appropriate for MND-S1, as the variation within a growth layer is as much as 1.5‰. With regards to the correlation along the growth axis, we point out that isotopic disequilibrium effects are not dominating the entire MND-S1 record since the disagreement between longer-term trends of  $\delta^{13}\text{C}$  and  $\delta^{18}\text{O}$  suggests underlying fractionation processes that are not common to both. In MND-S1, a shift in mean rainfall  $\delta^{18}\text{O}$  by processes that do not affect soil moisture and cave humidity significantly, such as a reduction in the number of large winter rainfall events, has the potential to affect speleothem  $\delta^{18}\text{O}$  but not  $\delta^{13}\text{C}$ . Given that the seasonal variation of speleothem  $\delta^{18}\text{O}$  (0.7–1.5‰) is much larger than the longer-term inter-decadal variation (0.3–0.5‰), even subtle changes in the amount of winter rainfall could potentially dominate the observed changes in mean speleothem  $\delta^{18}\text{O}$ . We compare speleothem  $\delta^{18}\text{O}$  with the rainfall record in detail below.

#### 4.5. Temporal trends in $\delta^{18}\text{O}$ and rainfall

The MND-S1 record for 1911–1992 shows two +0.3‰ shifts, one at 1930 and another post-1970, which could be simply explained by changing the frequency of intense events. The 0.3‰ rise in  $\delta^{18}\text{O}$  after 1970 is consistent with the rise in mean rainfall  $\delta^{18}\text{O}$  expected with the 20% decrease in regional rainfall which occurred at this time. The rainfall decrease is due to lower May–October rainfall (Fig. 9) attributed to a reduction in both the frequency and intensity of large events over the southwest region [37,38]. Mean precipitation-weighted  $\delta^{18}\text{O}$  falls from  $-4.3\text{‰}$  to  $-3.9\text{‰}$  if a single large event ( $-7.81\text{‰}$ , 38 mm, 29/09/01) is omitted from the lighthouse record demonstrating the sensitivity of annual rainfall  $\delta^{18}\text{O}$ , hence speleothem  $\delta^{18}\text{O}$ , to these large events. The 1911–1992 lighthouse rainfall record is unreliable, but we adopt the linear regression in Fig. 8 to convert the 1911–1992 daily rainfall records to  $\delta^{18}\text{O}$  for two high-quality stations [20]. We estimate that the rainfall decrease would raise annual rainfall  $\delta^{18}\text{O}$  by approximately 0.1‰ at Cape Naturaliste (Fig. 1) to 0.4‰ at Manjimup, with the latter being a minimum value as the lighthouse calibration does not account for overland isotopic distillation effects experienced by non-coastal sta-

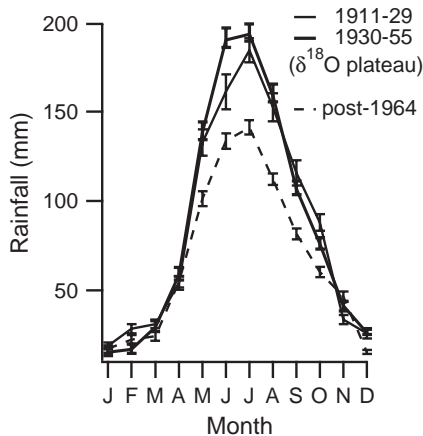


Fig. 9. Average annual cycles of mean monthly rainfall for the periods 1911–1929, 1930–1955 ( $\delta^{18}\text{O}$  plateau), and 1965–1992. 1930–1955 has higher rainfall in June compared with 1911–1929. This increase in early winter rain during 1930–1955 is due to the higher incidence of meridional troughs, which may bring  $^{18}\text{O}$ -enriched rainfall to the mid-latitudes of southwest Australia. The greatest decrease in rainfall post-1964 is for the winter months (May–October).

tions [22]. Moondyne Cave lies between these stations on the lee side of the coastal ridge. Thus the estimated change in rainfall  $\delta^{18}\text{O}$  is approximately equivalent to the rise in speleothem  $\delta^{18}\text{O}$  after 1970 and the record appears to have captured the rainfall decrease.

These arguments assume that the majority of calcite precipitated in each annual growth increment is sourced from May to September rainfall. However, the 0.7–1.5‰ annual cycles in speleothem  $\delta^{18}\text{O}$  revealed by ion microprobe analysis indicate that a significant amount of calcite is also sourced from isotopically heavier rainfall either from summer events or evaporation of soil water during warmer months [36]. If this is the case, then small changes in the relative masses of speleothem calcite deposited from isotopically light winter rainfall versus isotopically enriched rainfall/soil moisture could have produced the shifts in mean  $\delta^{18}\text{O}$  ( $\sim 0.3\text{‰}$ ), determined by bulk sampling of MND-S1, that have a complex relation to climate. For example, it is possible that the proportion of winter speleothem calcite could vary as a function of the carbonate saturation state of these waters. The post-1970 increase in speleothem  $\delta^{18}\text{O}$  may have also been

due to a reduction in calcite precipitated from May to September rainfall relative to the 1956–1970 period because there was less (isotopically light) winter rainfall overall (Fig. 9), and speleothem growth rates indicate that calcite is precipitated in narrower bands after 1970 (Fig. 7). On the other hand, we can account for the post-1970 rise in speleothem  $\delta^{18}\text{O}$  by the reduction of intense winter rainfall events alone.

A tendency for higher speleothem  $\delta^{18}\text{O}$  during drier periods does not hold for the 1930–1955 interval, as this was the longest wet period on record (Fig. 7). Whether this 0.3–0.5‰ increase in  $\delta^{18}\text{O}$  in the MND-S1 record can be attributed to either a change in the frequency of intense winter events or the mass of calcite deposited is difficult to assess. Averaged monthly rainfall for the periods 1911–1929 and 1930–1955 (Fig. 9) shows neither an increase in summer nor a decrease in winter rainfall during 1930–1955. However, the 1930–1955 period shows higher early winter rain (June; Fig. 9) than at any other period on record. Higher early winter rain during this period has been attributed to a higher incidence of meridional troughs [39]. The key link here may be that meridional troughs are capable of transporting tropical moisture, which is isotopically heavy, to the mid-latitudes.

Early and late winter rain vary slightly in their sources [39]. Southwesterly rain predominates over Moondyne Cave in winter, bringing moisture from nearby or higher latitudes. Northwesterly rain derived, in part, from the tropics is more common in late summer, but may extend to early winter [39]. Tropical moisture is isotopically heavier than that in higher latitudes [22] and may be transported to the mid-latitudes when meridional troughs link tropical and mid-latitude low pressure belts, reflecting the breakdown of the Australian summer monsoon. This process was observed in the Tasmanian rainfall  $\delta^{18}\text{O}$  dataset when an ‘east-coast low’ extends down the eastern Australian coast, bringing large amounts of rain with relatively high  $\delta^{18}\text{O}$  values [31]. In the southwest Australian rainfall dataset, several incidents involving meridional troughs were identified for May and June (dashed line, Fig. 4A) from mean sea-level pressure and cloud cover synoptic charts (not shown). But rainfall  $\delta^{18}\text{O}$  values for these events are not consistently higher

than those for other events with similar rainfall amounts, indicating that the contribution of a tropical moisture source is minimal. It thus appears unlikely that a persistent tropical moisture source could have raised rainfall  $\delta^{18}\text{O}$  over the period 1930–1955, but a much longer dataset of rainfall  $\delta^{18}\text{O}$  would be needed to confirm this.

A comparison of seasonal  $\delta^{18}\text{O}$  during the plateau (1930–1955), and before (1955–1970) and after the rainfall decrease (1970–1992), may have assisted the interpretation of the higher  $\delta^{18}\text{O}$  values seen in the conventional data. But it is highly unlikely that any differences would have been detectable outside the analytical precision. Furthermore, the +0.3–0.5‰ step in speleothem  $\delta^{18}\text{O}$  at 1930 coincides with an abrupt change in the calcite fabric from compact inclusion-free closed columnar calcite to inclusion-rich open columnar fabric (Fig. 2). The open nature of the crystallite fabric over this period is not suitable for ion microprobe analyses as a perfectly smooth surface is required to reduce topographic effects described earlier.

#### 4.6. Speleothem $\delta^{13}\text{C}$ temporal trends

Potential climatic effects on speleothem  $\delta^{13}\text{C}$  are not straightforward because speleothem  $\delta^{13}\text{C}$  begins to rise in 1938, 15 yr before temperature begins to rise and 27 yr before rainfall decreases. The 2.5‰ variation in  $\delta^{13}\text{C}$  is too large to be due to the effect of the 0.8 °C temperature rise on  $^{13}\text{C}/^{12}\text{C}$  fractionation [11,16]. A general response to the late 1960s decrease in rainfall may be evident if speleothem  $\delta^{13}\text{C}$  is divided into two episodes: (1) 1911–1955 when speleothem  $\delta^{13}\text{C}$  is at or below –9‰, and (2) post-1955 when the largest change in speleothem  $\delta^{13}\text{C}$  (+1.5‰) occurs, peaking at –8‰ in 1990. However, variations in speleothem  $\delta^{13}\text{C}$  are primarily a function of soil  $^{13}\text{CO}_2/^{12}\text{CO}_2$ , and  $\text{CO}_2$  degassing rate if the difference in the partial pressures of  $\text{CO}_2$  between the solution and cave atmosphere is large [11]. Therefore, we examine all possible impacts of the environmental history on soil  $^{13}\text{CO}_2/^{12}\text{CO}_2$  above Moondyne Cave during the growth of MND-S1.

Speleothem  $\delta^{13}\text{C}$  values during the 1911–1955 interval are close to values modelled [11,16] for drip water that has not degassed significantly before

reaching the speleothem. This suggests that the speleothem  $\delta^{13}\text{C}$  variations broadly represents the cumulative fractions of  $^{13}\text{C}/^{12}\text{C}$  in the soil carbon pool above the cave. The lowering of speleothem  $\delta^{13}\text{C}$  during ~1927–1953 suggests that it is responding to the wetter climate at this time. A possible driver of this ~1‰ decrease in  $\delta^{13}\text{C}$  may be an increase in the partial pressure of soil  $\text{CO}_2$  during wetter years if limestone dissolution is taking place under open-system conditions, but this is speculative.

Recent studies have found large (more than several per mil) fluctuations in speleothem  $\delta^{13}\text{C}$  in modern [28] and Pleistocene [40] speleothems that were attributed to an increase in the relative proportion of  $^{13}\text{C}$ -enriched atmospheric  $\text{CO}_2$  to  $^{13}\text{C}$ -depleted biogenic  $\text{CO}_2$  in the soil carbon pool. It is possible that the thickening of understory C3-type vegetation due to a reduction in regional forest burning may have altered the  $\delta^{13}\text{C}$  of soil  $\text{CO}_2$ . However, if it did, we would expect to see a post-1970 decrease in speleothem  $\delta^{13}\text{C}$  owing to an increase in  $^{13}\text{C}$ -depleted biogenic soil  $\text{CO}_2$ . If the burning itself affected speleothem  $\delta^{13}\text{C}$  values, either through vegetation loss or change to the  $^{13}\text{C}/^{12}\text{C}$  of the decaying matter, then we would expect our conventional  $\delta^{13}\text{C}$  analyses, which typically span 1–3 yr growth, to capture this, but we do not see significant short-term effects. Similarly, we cannot attribute the rise in speleothem  $\delta^{13}\text{C}$  to C4-type plants with metabolic pathways that favour the uptake of  $^{13}\text{C}$  [3]. Grasses make up a minor portion of the vegetation covering Moondyne Cave and only 20% of southwest Australian grasses use the C4 pathway [41]. If C4 grasses were present within a thinned understory, they were replaced by thick woody C3-type vegetation from about 1980 onwards, which would drive soil  $^{13}\text{CO}_2/^{12}\text{CO}_2$  in the opposite sense. Other studies have tracked the reduction in atmospheric  $^{13}\text{CO}_2/^{12}\text{CO}_2$  due to fossil fuel burning in modern speleothems [42], but this is clearly not dominating our record.

Water stress may also raise the  $^{13}\text{C}/^{12}\text{C}$  ratio of biogenic  $\text{CO}_2$  by contracting leaf stomata, thus restricting  $\text{CO}_2$  supply [13,14]. A survey of leaf  $\delta^{13}\text{C}$  in vegetation dominated by *Eucalyptus*, *Acacia*, and *Melaleuca* species along a rainfall gradient in southern Queensland indicated an approximate 1‰ increase in  $\delta^{13}\text{C}$  for every 200 mm decrease in rainfall [43], consistent with the observed changes in the

MND-S1 speleothem and southwest Australian meteorological records after the late 1960s.

We consider also that water reduction may also bring about kinetic fractionation of  $^{13}\text{C}/^{12}\text{C}$  in the precipitating solution also, argued as follows. During the drier 1956–1992 interval, the increase in speleothem  $\delta^{13}\text{C}$  parallels the increase in speleothem Mg (Fig. 7), which was interpreted to reflect the longer residence time of water in the overlying limestone due to a reduction in rainfall recharge. The primary mechanism for an increase in the Mg/Ca ratio in MND-S1 during the prolonged drier period was interpreted to be prior-calcite precipitation resulting in a loss of Ca with continual uptake of Mg, once the water has reached saturation with respect to Ca [44]. Since this process implies that calcite is precipitated before reaching the speleothem, it also indicates that degassing of  $\text{CO}_2$  from the saturated waters must have occurred, which will increase drip water  $\delta^{13}\text{C}$  [12]. The Pearson's correlation coefficient between  $\delta^{13}\text{C}$  and Mg (when averaged to approximately the same sampling resolution of  $\delta^{13}\text{C}$ ) is weak ( $r=+0.29$ ,  $p<0.03$ ), indicating that some other process is contributing, whether this be  $^{13}\text{C}$  enrichment of soil organic matter or isotopic disequilibrium processes.

Isotopic disequilibrium precipitation processes are controlled by the rate of  $\text{CO}_2$  degassing from the solution, but we cannot identify any event in the history of Moondyne Cave that could have brought about a change in either solution  $\text{CO}_2$  partial pressure or cave atmosphere partial pressure at this time, since rainfall, temperature, and vegetation did not alter significantly until after 1964–1970, nor cave use until 1959. Nonetheless, the short-term covariation between  $\delta^{13}\text{C}$  and  $\delta^{18}\text{O}$  is very strong, indicating that isotopic disequilibrium processes are important in MND-S1, but dominate sub-decadal rather than longer-term variations.

## 5. Conclusions

In situ ion microprobe analysis of  $\delta^{18}\text{O}$  annual cycles in stalagmite MND-S1 demonstrates that seasonal variations of  $\delta^{18}\text{O}$  of rainfall are preserved in southwest Australian speleothems. Our findings suggest that analysis of annual  $\delta^{18}\text{O}$  cycles in speleothems from shallow sites, where the seasonal

rainfall  $\delta^{18}\text{O}$  signal passes through the cave roof, could be a powerful tool for the reconstruction of rainfall variability over short timescales. However, conventional  $\delta^{13}\text{C}$  and  $\delta^{18}\text{O}$  analyses of the entire speleothem record (1911–1992) show isotopic trends that cannot be readily reconciled with the instrumental meteorologic record. The lack of simple responses of speleothem  $\delta^{18}\text{O}$  and  $\delta^{13}\text{C}$  to either climate or non-climate factors on decadal timescales calls for investigation of another active speleothem from the same area, keyed to the results reported here by using annual trace element cycles. This is a key aim of ongoing research and will confirm how robust the response of southwest Australian speleothems is to the rainfall decrease. Drip water and continued rainfall monitoring will enable full examination of the isotopic signature of meridional troughs.

For now, the seasonal variation in speleothem  $\delta^{18}\text{O}$  revealed by ion microprobe analysis indicates that subtle changes in the frequency of intense winter rainfall events and possibly moisture sources could produce significant changes in mean speleothem  $\delta^{18}\text{O}$ . The ion microprobe results also raise the possibility that the masses of speleothem calcite deposited in winter and summer could vary as a function of the seasonal drip rate and carbonate saturation state of these waters. If this is the case, then small changes in the relative masses of calcite deposited in winter and summer could produce significant shifts in mean  $\delta^{18}\text{O}$  and  $\delta^{13}\text{C}$  that have a complex relation to climate. These findings should be generally applicable to the interpretation of long-term trends in speleothem geochemical records for shallow caves where seasonal variations in geochemical tracers are relatively large, including the sub-tropical monsoon belts and mid to high latitudes with distinct rainfall seasons.

## Acknowledgements

We thank Caveworks (Margaret River, WA) for loan of MND-S1 and their assistance, N. Nicholls for the instrumental climate dataset, and S. Eberhard for Moondyne Cave's history. We also thank Marty Grove, Joe Cali, Mike Shelley, and Heather Scott-Gagan for technical assistance; Graham Farquhar and Hilary Stuart-Williams for water analyses at RSBS; Joan Cowley for water  $\delta^{18}\text{O}$  analyses at RSES; and

Silvia Frisia, Ian Fairchild, and Christoph Spötl for helpful comments. P.T. acknowledges financial support from an Australian Postgraduate Award and RSES, ANU. Ion microprobe measurements were funded by the USA Department of Energy grant DE-FG-03-89ER14049 and the instrumentation and facilities of NSF grant EAR-0113563.

## References

- [1] C. Henny, A. Wilson, Palaeoclimatic data from speleothems, *Nature* 219 (1968) 48–51.
- [2] A. Goede, Continuous early last glacial palaeoenvironmental record from a Tasmanian speleothem based on stable isotope and minor element variations, *Quat. Sci. Rev.* 13 (1994) 283–291.
- [3] J.A. Dorale, R.L. Edwards, E. Ito, L.A. Gonzalez, Climate and vegetation history of the midcontinent from 75 to 25 ka: a speleothem records from Crevice Cave, Missouri, USA, *Science* 282 (1998) 1871–1874.
- [4] M. Bar-Matthews, A. Ayalon, A. Kaufman, G.J. Wasserburg, The Eastern Mediterranean paleoclimate as a reflection of regional events: Soreq Cave, Israel, *Earth Planet. Sci. Lett.* 166 (1999) 85–95.
- [5] F. McDermott, D.P. Matthey, C. Hawkesworth, Centennial-scale Holocene climate variability revealed by a high-resolution speleothem  $\delta^{18}\text{O}$  record from SW Ireland, *Science* 294 (2001) 1328–1330.
- [6] Y.J. Wang, H. Cheng, R.L. Edwards, Z.S. An, J.Y. Wu, C.C. Shen, J.A. Dorale, A high-resolution absolute dated late Pleistocene monsoon record from Hulu Cave, China, *Science* 294 (2001) 2345–2348.
- [7] C. Spötl, A. Mangini, Stalagmite from the Austrian Alps reveals Dansgaard–Oeschger events during isotope stage 3: implications for the absolute chronology of Greenland ice cores, *Earth Planet. Sci. Lett.* 203 (2002) 507–518.
- [8] P.F. Dennis, P.J. Rowe, T.C. Atkinson, The recovery and isotopic measurement of water from fluid inclusions in speleothems, *Geochim. Cosmochim. Acta* 65 (2001) 871–884.
- [9] H. Dorr, K. Munnich, Annual variations of the  $^{14}\text{C}$  content of soil  $\text{CO}_2$ , *Radiocarbon* 28 (1986) 338–345.
- [10] C. Henny, The use of  $^{14}\text{C}$  in the study of cave processes, *Nobel Symp.* (1970) 419–443.
- [11] C. Henny, The isotope geochemistry of speleothems I. The calculation of the effects of different modes of formation on the isotopic composition of speleothems and their applicability as palaeoclimatic indicators, *Geochim. Cosmochim. Acta* 35 (1971) 802–824.
- [12] A. Baker, E. Ito, P. Smart, R. McEwan, Elevated and variable values of  $^{13}\text{C}$  in speleothems in a British cave system, *Chem. Geol.* 136 (1997) 263–270.
- [13] L.L. Tieszen, T.W. Boutton, Stable carbon isotopes in terrestrial ecosystem research, in: P.W. Rundel, J.R. Ehleringer, K.A. Nagy (Eds.), *Stable Isotopes in Ecological Research*, Springer-Verlag, New York, 1989, pp. 167–195.
- [14] G.D. Farquhar, K.T. Hubrick, A.G. Condon, R.A. Richards, Carbon isotope fractionation and plant water-use efficiency, in: P.W. Rundel, J.R. Ehleringer, K.A. Nagy (Eds.), *Stable Isotopes in Ecological Research*, Springer-Verlag, New York, 1989, pp. 21–40.
- [15] T. Cerling, The stable isotope composition of modern soil carbonate and its relationship to climate, *Earth Planet. Sci. Lett.* 71 (1984) 229–240.
- [16] M. Dulinski, K. Rozanski, Formation of  $^{13}\text{C}/^{12}\text{C}$  isotope ratios in speleothems: a semi-dynamic model, *Radiocarbon* 32 (1990) 7–16.
- [17] A.C. Kendall, P.L. Broughton, Origin of fabrics in speleothems composed of columnar calcite crystals, *J. Sediment. Petrol.* 48 (1978) 519–538.
- [18] P. Treble, J. Shelley, J. Chappell, Comparison of high-resolution sub-annual records of trace elements in a modern (1911–1992) speleothem with instrumental climate data from southwest Australia, *Earth Planet. Sci. Lett.* 216 (2003) 141–153.
- [19] R.M. Hocking, A.E. Cockbain, *Regolith, Geology and Mineral Resources of Western Australia*, Memoir, vol. 3, Geol. Soc. West. Aust., Perth, 1990, pp. 601–602.
- [20] B. Lavery, A. Kariko, N. Nicholls, A historical rainfall data set for Australia, *Aust. Meteorol. Mag.* 40 (1992) 33–39.
- [21] R.J. Allan, M.R. Haylock, Circulation features associated with the rainfall decrease in south-western Australia, *J. Clim.* 7 (1993) 1356–1367.
- [22] K. Rozanski, L. Araguas-Araguas, R. Gonfiantini, Isotopic patterns in modern global precipitation, in: P.K. Swart, K.C. Lohmann, J. McKenzie, S. Savin (Eds.), *Climate Change in Continental Isotopic Records*, Am. Geophys. Union, Washington, 1993, pp. 1–36.
- [23] G.D. Farquhar, B.K. Henry, J.M. Styles, A rapid on-line technique for determination of oxygen isotope composition of nitrogen-containing organic matter and water, *Rapid Commun. Mass Spectrom.* 11 (1997) 1554–1560.
- [24] S.R. Epstein, T. Mayeda, Variations of  $^{18}\text{O}$  content of waters from natural sources, *Geochim. Cosmochim. Acta* 4 (1953) 213–224.
- [25] R.A. Socki, H.R. Karlsson, E.K. Gibson Jr., Extraction technique for the determination of oxygen-18 in water using pre-evacuated glass vials, *Anal. Chem.* 64 (1992) 829–831.
- [26] M.K. Gagan, A.R. Chivas, P.J. Isdale, High-resolution isotopic records from corals using ocean temperature and mass-spawning chronometers, *Earth Planet. Sci. Lett.* 121 (1994) 549–558.
- [27] J.M. McCrea, On the isotopic chemistry of carbonates and a paleotemperature scale, *J. Chem. Phys.* 18 (1950) 849–857.
- [28] A. Frappier, D. Sahagian, L.A. Gonzalez, S.J. Carpenter, El Niño events recorded by stalagmite carbon isotopes, *Science* 298 (2002) 565.
- [29] P.C. Treble, Palaeoclimate records constructed from southern Australian modern, Holocene and Pleistocene speleothems. PhD Thesis, Australian National University, Canberra, 2003, 224 pp.
- [30] Y. Kolodny, M. Bar-Matthews, A. Ayalon, K.D. McKeegan, A high spatial resolution  $\delta^{18}\text{O}$  profile of a speleothem using an ion-microprobe, *Chem. Geol.* 197 (2003) 21–28.

- [31] P.C. Treble, W.F. Budd, P.K. Hope, P.K. Rustomji, Synoptic-scale climate patterns associated with rainfall  $\delta^{18}\text{O}$  in southern Australia, *J. Hydrol.* 302 (2005) 270–282.
- [32] S.D. Gedzelman, J.R. Lawrence, The isotopic composition of precipitation from two extratropical cyclones, *Mon. Weather Rev.* 118 (1999) 495–509.
- [33] J.W. Valley, C.M. Graham, Ion microprobe analysis of oxygen isotope ratios in granulite facies magnetites: diffusive exchange as a guide to cooling history, *Contrib. Mineral Petrol.* 109 (1991) 38–52.
- [34] J.R. O'Neil, R.N. Clayton, T.K. Mayeda, Oxygen isotope fractionation in divalent metal carbonates, *J. Chem. Phys.* 31 (1969) 5547–5558.
- [35] A. Goede, D.C. Green, R.S. Harmon, Isotopic composition of precipitation, cave drips and actively forming speleothems at three Tasmanian cave sites, *Helveticite* 19 (1982) 57–67.
- [36] A. Ayalon, M. Bar-Matthews, E. Sass, Rainfall–recharge relationships within a karstic terrain in the Eastern Mediterranean semi-arid region, Israel:  $\delta^{18}\text{O}$  and dD characteristics, *J. Hydrol.* 207 (1998) 18–31.
- [37] M. Haylock, N. Nicholls, Trends in extreme rainfall indices for an updated high quality data set for Australia, 1910–1998, *Int. J. Climatol.* 20 (2000) 1533–1541.
- [38] I. Simmonds, K. Keay, Variability of Southern Hemisphere extratropical cyclone behaviour, 1958–97, *J. Clim.* 13 (2000) 550–561.
- [39] P.B. Wright, Seasonal rainfall in southwestern Australia and the general circulation, *Mon. Weather Rev.* 102 (1974) 219–233.
- [40] D. Genty, D. Blamart, R. Ouahdi, M. Gilmour, A. Baker, J. Jouzel, S. Van-Exter, Precise dating of Dansgaard–Oeschger climate oscillations in western Europe from stalagmite data, *Nature* 421 (2003) 833–837.
- [41] P.W. Hattersley, The distribution of C3 and C4 grasses in Australia in relation to climate, *Oecologia* 57 (1983) 113–128.
- [42] D. Genty, M. Massault, Carbon transfer dynamics from bomb- $^{14}\text{C}$  and  $\delta^{13}\text{C}$  time series of a laminated stalagmite from SW France—modelling and comparison with other stalagmite records, *Geochim. Cosmochim. Acta* 63 (1999) 1537–1548.
- [43] G.R. Stewart, M.H. Turnbull, S. Schmidt, P.D. Erskine,  $^{13}\text{C}$  natural abundance in plant communities along a rainfall gradient: a biological integrator of water availability, *Aust. J. Plant Physiol.* 22 (1995).
- [44] I.J. Fairchild, A. Borsato, A.F. Tooth, S. Frisia, C.J. Hawkesworth, Y. Huang, F. McDermott, B. Spiro, Controls on trace element (Sr–Mg) compositions of carbonate cave waters: implications for speleothem climatic records, *Chem. Geol.* 166 (2000) 255–269.